Performance Improvement Techniques in Shell-and-Tube Type of LHS Unit

Berihu Gebreyohannes Abreha, Pinakeswar Mahanta, and Gaurav Trivedi

Nomenclature

A_{Mush}	Mushy region constant value
Cp	Specific heat capacity (J kg^{-1} K^{-1})
F	Body force (N m^{-3})
g	Acceleration due to gravity (m s^{-2})
h	Specific enthalpy (J/kg)
L	Latent heat of fusion (J kg^{-1})
k	Thermal conductivity (W m^{-1} K^{-1})
P	Pressure (Pa)
S	Darcy law's source term
T	Temperature (K)
v	Velocity (m/s)

Greek Symbols

ρ	Density (kg/m^3)

B. G. Abreha
Center for Energy, Indian Institute of Technology Guwahati, Guwahati, Assam 781039, India

P. Mahanta (✉)
Department of Mechanical Engineering, Indian Institute of Technology Guwahati, Guwahati, Assam 781039, India
e-mail: pinak@iitg.ac.in

National Institute of Technology Arunachal Pradesh, Yupia, Arunachal Pradesh 791112, India

G. Trivedi
Department of Electronics and Electrical Engineering, Indian Institute of Technology Guwahati, Guwahati, Assam 781039, India

P. Mahanta et al. (eds.), *Advances in Thermofluids and Renewable Energy*, Lecture Notes in Mechanical Engineering, https://doi.org/10.1007/978-981-16-3497-0_12

β	Coefficient of thermal expansion (1/K)
μ	Dynamic viscosity (Ns/m^2)
θ	Melt fraction
φ	Nanoparticles volume fraction

Subscripts

ini	Initial
l	Liquid
np	Nanoparticle
nPCM	Nanophase change material
s	Solid
Ref	Reference

1 Introduction

Fossil fuel is the primary energy source to fulfill the ongoing increase in global energy demand. Increasing the share of renewable energy, such as solar energy in the energy mix is a very important step to alleviate environmental hazards and energy security problems. However, renewable energy sources are intermittent and unpredictable in nature. Thus, storing solar energy is necessary to maintain a continuous supply of energy and to satisfy the demand of end users [1].The difference between energy supply and demand can be minimized by developing effective energy storage technologies. Generally speaking, thermal energy storage systems are of three kinds, viz. sensible heat storage (SHS), latent heat storage (LHS), and chemical heat storage system [2]. Latent heat type storage device is considered more efficient and highly compacted, and due to these attractive properties, LHS is preferred frequently [3].

However, the latent thermal energy system suffers from poor thermal conductivity, and this is a critical problem that results in low charging and discharging rates of PCM [4]. Consequently, several effective thermal conductivity enhancement techniques have been practiced including embedding fins into the PCM [5], inserting metal matrix or carbon foams [6, 7], dispersing nanoparticles and carbon-based particles embedded in PCM [8], etc.

A comprehensive examination of the heat transfer characteristics between HTF and PCM is essential to design and develop the most effective storage unit. For the selection of the most efficient and economically affordable TES unit, conducting optimization techniques is important. This is a difficult task considering the cost and performance criteria of the storage unit. For optimal design and material selection of TES numerical modeling of the LHS system is a perfect solution to overcome the above mentioned problem. From the aforementioned reviewed literature, it is

observed that there is a lack of investigations undertaken on a comparison study of various performance enhancement techniques of shell-and-tube LHS unit. Hence, the principal objective of this paper is to perform a performance comparative study of three shell-and-tube type LHS units using erythritol as PCM.

2 Numerical Formulation

In this section, the geometric characteristics of the selected LHS units are described. Moreover, the governing equations that are used to solve the phase transition characteristics of the PCM are formulated, and the material properties of the domains considered in the numerical investigation are also defined. In addition, the grid size and boundary conditions are explained in this section.

2.1 Model Description

Figure 1 represents three physical modeling diagram of shell-and-tube LHS units considered for this study. With the help of an optimization technique, 19 tubes are selected with an internal and external diameter of 17 mm and 20 mm, respectively. The shell of the LHS unit illustrated in Fig. 1a is filled with PCM. In the second case, the LHS model is also modeled without fins, but the phase changing materials (PCM) are mixed with 5% volume fraction of Cu nanoparticles and is exhibited in Fig. 1b. In the third case, each HTF tube is supported by four longitudinal fins to improve the heat transfer penetration from the hot walls into PCM and is presented in Fig. 1c. In order to maintain the same volume of PCM in all models, the container diameter of the LHS models is kept different. The internal shell diameter of the storage unit in the first case is 235 mm. On the other hand, the internal shell diameters of the second and third models of LHS units are the same and it is set to be 240 mm. In case two, 5% of the volume of the shell is contained by the Cu nanoparticles and this is equal to the volume of the fins in case three. Because of superior thermal conductivity, HTF pipes and fins are considered to be of copper material and, width and thickness of each fin are chosen as 12 mm and 2 mm, respectively. Commercial sugar alcohol known as erythritol ($C_4H_{10}O_4$) is considered as PCM. The thermal properties of PCM and copper are presented in Table 1.

2.2 Thermal Properties of Materials

The thermal properties of the nano-PCM (a mixture of PCM and nanoparticle) are derived from the respective volume fraction of nanoparticle and PCM considering

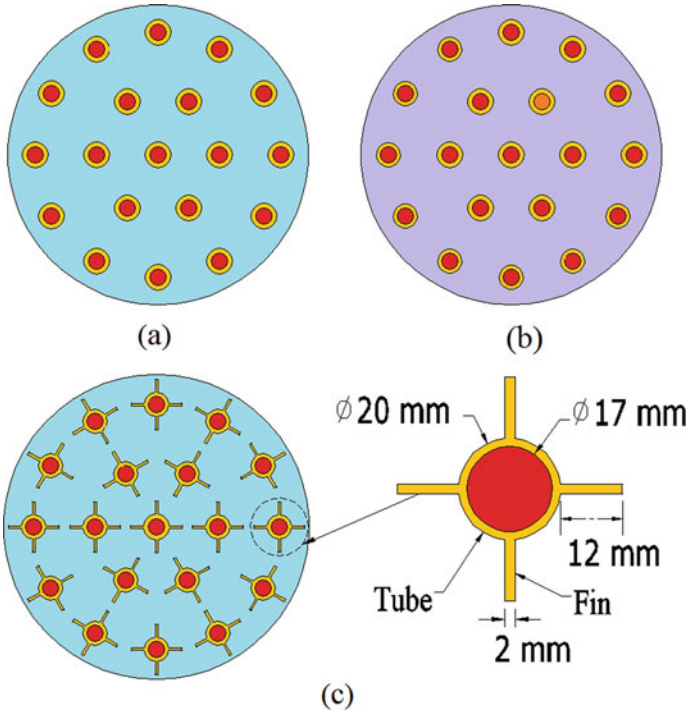

Fig. 1 Physical modeling diagram of shell-and-tube LHS units consider for this study

Table 1 Thermophysical properties of erythritol and copper [7, 10–12]

Properties	Erythritol	Copper
ρ (kg/m^3)	1450 (S)	8978
	1280 (L)	
C_p(J/kgK)	1680 (S)	381
	2660 (L)	
K (W/m K)	0.73 (S)	387.6
	0.33 (L)	
L (kJ/kg)	354.7	
T_m (°C)	118	
μ(kg/ms)	$1.6 \times 10{-}^2$	
$\beta(K^{-1})$	$2.94 \times 10{-}^5$	

the theoretical mixing and are listed below [9]. The thermosphysical properties of nano-PCM are also listed in Table 1.

Density

$$\rho_{n,\mathrm{PCM}} = \varphi_n \rho_{\mathrm{np}} + (1 - \varphi_n)\rho_{\mathrm{PCM}} \tag{1}$$

Specific heat capacity

$$C_{P,\text{npcm}} = \frac{\varphi_n\left(\rho_{\text{np}} C_{P,\text{np}}\right) + (1-\varphi_n)(C_P\rho)_{\text{PCM}}}{\rho_{n,\text{PCM}}} \tag{2}$$

Latent heat

$$L_{n,\text{PCM}} = \frac{(1-\varphi_n)(\rho L)_{\text{PCM}}}{\rho_{n,\text{PCM}}} \tag{3}$$

Thermal expansion coefficient

$$\beta_{n,\text{PCM}} = \frac{\varphi_n(\rho\beta)_{\text{np}} + (1-\varphi_n)(\beta\rho)_{\text{PCM}}}{\rho_{n,\text{PCM}}} \tag{4}$$

The effective dynamic viscosity of nano-PCM can be calculated as follows [13].

$$\mu_{n,\text{PCM}} = 0.983\text{e}^{(12.959\varphi_n)}\mu_{\text{PCM}} \tag{5}$$

The effective thermal conductivity of the mixture of nanoparticle and PCM is described with the help of Maxwell's theory and Brownian motion [14].

$$k_{n,\text{PCM}} = \frac{k_{\text{np}} + 2k_{\text{PCM}} - 2*\varphi_n\left(k_{\text{PCM}} - k_{\text{np}}\right)}{k_{\text{np}} + 2k + \varphi_n\left(k_{\text{PCM}} - k_{\text{np}}\right)} k_{\text{PCM}} \tag{6}$$

2.3 Thermal Modeling

In this study, a two-dimensional CFD model has been built to analyze the melting performance of LHS units using computational fluid dynamics (CFD) ANSYS Fluent software. For modeling the phase transition of PCM, the commonly used enthalpy–porosity technique is applied, and this method helps to combine enthalpy with the temperature jointly as a function presented below. The numerical model is developed using Navier–Stokes equations that define the conservation of mass, momentum, and energy. For the buoyancy entity inside the momentum equation, density gradients are handled using Boussinesq approximation [15].

The next assumptions are taken into account in the numerical formulation to evaluate the performance of storage unit. The PCM and nanoparticles are mixed uniformly; the flow is assumed to be laminar, incompressible, and unsteady. The viscous and dissipation term is also assumed to be negligible. The PCM and HTF tubes have steady reference temperature, and the storage system is assumed to be thermally insulated to ensure that there is no heat loss toward external wall of the PCM.

Continuity equation

$$\frac{\partial \rho}{\partial t} = \nabla.\left(\rho \vec{V}\right) \tag{7}$$

Momentum conservation equation

$$\rho \frac{\partial \vec{V}}{\partial t} + \rho \vec{V}.\left(\nabla.\vec{V}\right) = -\nabla P + \mu \nabla^2 \vec{V} + \rho \beta \vec{g}(T - T_{\text{ref}}) + \vec{S} \tag{8}$$

Energy conservation equation

$$\frac{\partial}{\partial t}(\rho h) + \nabla.\left(\rho.\vec{V}h\right) = \nabla(k \nabla T) \tag{9}$$

The overall enthalpy (H) is equal to the sum of sensible enthalpy (h) and latent heat (ΔH), which is resulted due to phase conversions.

$$H = h + \Delta H \tag{10}$$

where,

$$h = h_{\text{e}} + \int_{T_{\text{ref}}}^{T} C_{\text{p}} \text{d}T \tag{11}$$

$$\Delta H = \theta L \tag{12}$$

The movement of PCM solid–liquid interface is tracked by enthalpy–porosity method. To monitor liquid part in the mushy region, a liquid fraction parameter is introduced in the enthalpy–porosity technique. The liquid fraction (θ) of each cell represents porosity of that given cell. The solid region has no porosity and its liquid fraction is zero. The melting front of PCM is considered as a mushy region having a liquid fraction value that spans between 0 and 1. Normally, melting fraction (θ) of PCM can be expressed as Eq. (13).

$$\theta = \frac{\Delta H}{L} = \begin{cases} 0 & \text{if } T < T_{\text{s}} \\ \frac{T - T_{\text{s}}}{T_l - T_{\text{s}}} & \text{if } T_{\text{s}} < T < T_l \\ 1 & \text{if } T > T_{\text{l}} \end{cases} \tag{13}$$

The source term $\vec{S}$, which is added in the momentum conservation equation, is defined as:

$$\vec{S} = \frac{(1 - \theta)^2}{\left(\theta^3 + \varepsilon\right)} A_{\text{Mush}} \vec{V} \tag{14}$$

where, ε is an insignificant quantity (10^{-3}) placed to avoid division by zero. The mushy region's constant value lies between 10^4 and 10^7, and is frequently applied for computations, and the value for this study is set equal to 105 [16]. All the cases of LHS are tested with three different meshes sizes to examine dependency on grid size and time step size. This helps in deciding an optimal size considering both accuracy and time. The variations between finer and extra fine mesh outcomes are insignificant. Hence, finer mesh has been selected for the simulation of all the LHS models. The mesh elements size of first, second, and third LHS models are 11,031, 15,728, and 20,931, respectively. In all the cases, initial temperature of the entire system is 20 °C, and there is no heat loss from external walls. The inlet temperature of the HTF is set as 138 °C.

3 Results and Discussion

The governing equations that are formulated in Section 2 are solved using CFD software. The transient temperature and liquid fraction parameters are employed to evaluate the performances of selected storage units. Due to the symmetrical half of LHS, models are considered for the numerical analysis. The time taken for the entire melting of PCM inside the storage unit is related to the rate of temperature increase. In order to ensure that the numerical results are correct and reliable, the experimental study of Agyenim et al. [17] has been solved numerically using the same numerical setup, which is utilized for the current study.

The same properties of PCM and, similar initial and boundary conditions of the experimental study are employed for the validation. The timewise temperature parameter during the charging process is used for the comparison of these two studies.

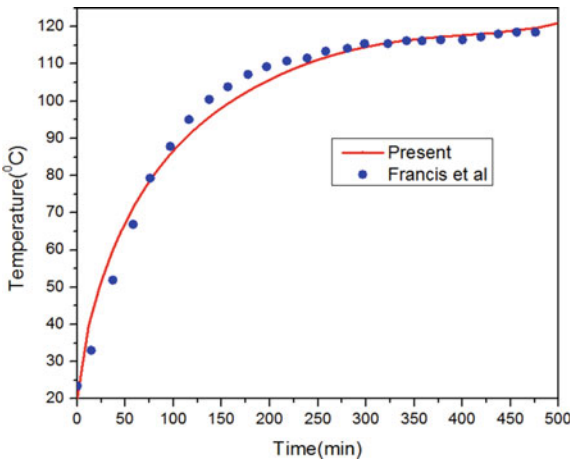

Fig. 2 Comparison of present study versus Agyenim et al. [17] results

Figure 2 illustrates the numerical and practical results, and a good agreement is observed between them.

Figure 3 depicts the variations of average temperature versus time of three LHS units during the charging process. It can be noticed that the temperature curves of all the models are becoming steeper up to 10 min without significant difference among them. This could be resulted due to the dominant conduction heat transfer in all the cases near the beginning of the process. Later, the rate of heat addition in the finned LHS unit is found to be higher than the other two. This is because of the better heat transfer in the finned LHS unit due to the extended surface of the fins. Due to the uniformly distributed fins, the temperature expansion is more uniform and highest as compared with LHS models without fins and the LHS unit with nano-PCM. Even though the thermal conductivity of PCM in the second LHS model is improved by adding 5% volume fraction Cu nanoparticle, the heat transfer rate is even slower than the first model. The internal shell diameter of the first model is smaller as compared to the other models. Hence, the outward heat transfer from the wall of HTF tubes of the LHS model with nano-PCM is delayed as compared to the first model. As it is explained above, the temperature of finned LHS unit increases more quickly, and since its magnitude is reached 137.8 °C at at 80 min, which is almost same as the inlet temperature of HTF tubes.

The liquid fraction variation as a function of time for all LHS units is shown in Fig. 4. It can be seen from this figure that the finned LHS has a constant increase in the melt fraction than the LHS model without fins. As it is expected, the melting progress of the PCM in the finned LHS unit is faster. From the beginning of the charging process, there is a noticeable difference in the melting progress in the finned LHS among all the storage systems. The presence of fins in the HTF tubes augments the heat transfer across the storage unit and improves thermal conductivity of the PCM.

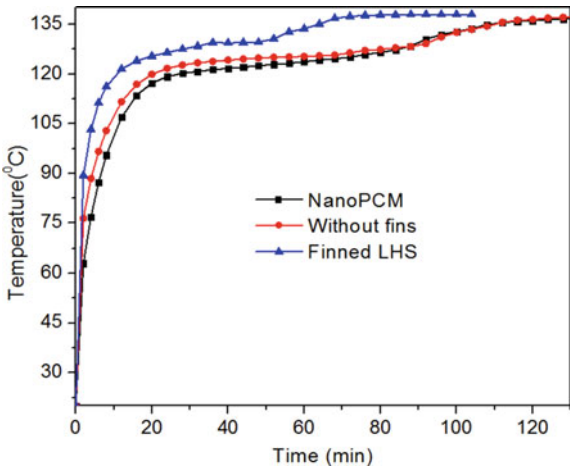

Fig. 3 Transient temperature comparison of the LHS units

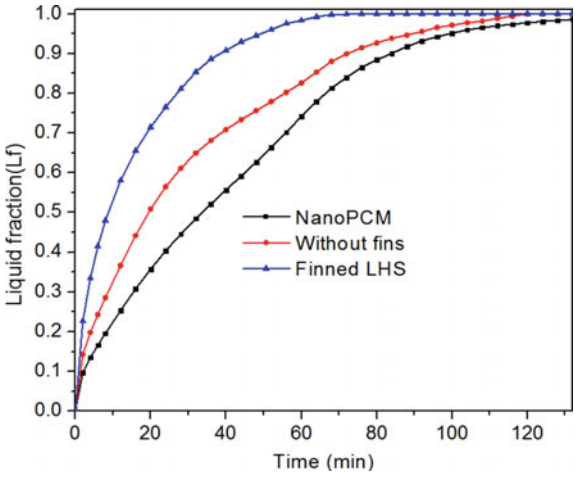

Fig. 4 Transient liquid fraction comparison of the LHS units

In this context, the total time taken for the complete melting of PCM in the finned LHS unit is 80 min, whereas the LHS models in the first and second cases consume 120 and 136 mins, respectively. As a result, the third LHS model supported by fins has been found the best option to be used in various applications.

4 Conclusion

This study presents a comparative study of the thermal performances of three shell-and-tube LHS models. With the help of an optimization technique, 19 tubes are selected with an internal and external diameter of 17 mm and 20 mm, respectively for the proposed study. In the first case, LHS is considered without fins.

In the second case, LHS is also modeled without fins, but the phase changing materials (PCM) are mixed with 5% volume fraction of Cu nanoparticles. In the third case, every HTF tube is supported by four fins. In order to maintain the same volume of PCM in all the models, the shell diameter of the first LHS model is 235 mm and, for the second and third cases, the diameter is set to be 240 mm. Erythritol ($C_4H_{10}O_4$) is considered as PCM in this study. The thermal performance of LHS is evaluated numerically and charging time, liquid fraction, transient temperature, and stored energy are estimated. The buoyancy effect of liquid PCM is modeled using Boussinesq approximation method in the proposed study.

The outcome of numerical analysis is validated with the experimental results to ensure reliability of the proposed work. It is observed that the temperature of finned LHS unit increases quickly. The LHS in the third case gets fully charged after 80 min, whereas LHSs in the first and second cases take 120 and 136 min, respectively, for complete melting. This exhibits that the third LHS model supported by fins is the

best option for getting it utilized in various applications, such as hybrid solar cooker etc.

References

1. Herrmann, U., & Kearney, D. W. (2002). Survey of thermal energy storage for parabolic trough power plants. *The Journal of Solar Energy Engineering Transfer ASME, 124*(2), 145–152.
2. Gil, et al. (2010). State of the art on high temperature thermal energy storage for power generation. Part 1-Concepts, materials and modellization. *Renewable and Sustainable Energy Reviews, 14*(1), 31–55.
3. Ghoneim, A. (1989). The effect of phase-change material properties on the performance of solar air-based heating systems. *Solar Energy, 42*(6).
4. Regin, F., Solanki, S. C., & Saini, J. S. (2008). Heat transfer characteristics of thermal energy storage system using PCM capsules: A review. *Renewable and Sustainable Energy Reviews, 12*(9), 2438–2458.
5. Niyas, H., Prasad, S., & Muthukumar, P. (2017). Performance investigation of a lab–scale latent heat storage prototype—Numerical results. *Energy Conversion and Management, 135*, 188–199.
6. Zhao, Y., Lu, W., & Tian, Y. (2010). Heat transfer enhancement for thermal energy storage using metal foams embedded within phase change materials (PCMs). *Solar Energy, 84*(8), 1402–1412.
7. Wang, W., He, S., Guo, S., Yan, J., & Ding, J. (2014). A combined experimental and simulation study on charging process of Erythritol-HTO direct-blending based energy storage system. *Energy Conversion and Management, 83*, 306–313.
8. Owolabi, L., Al-Kayiem, H. H., & Baheta, A. T. (2016). Nanoadditives induced enhancement of the thermal properties of paraffin-based nanocomposites for thermal energy storage. *Solar Energy, 135*, 644–653.
9. Khan, Z., Khan, Z., & Tabeshf, K. (2016). Parametric investigations to enhance thermal performance of paraffin through a novel geometrical configuration of shell and tube latent thermal storage system. *Energy Conversion and Management, 127*, 355–365.
10. Nomura, T., Okinaka, N., & Akiyama, T. (2009). Impregnation of porous material with phase change material for thermal energy storage. *Materials Chemistry and Physics, 115*(2–3), 846–850.
11. Fasina, O. O., & Colley, Z. (2008). Viscosity and specific heat of vegetable oils as a function of temperature: 35 °C to 180 °C. *International Journal of Food Properties, 11*(4), 738–746.
12. Al-Abidi, A., Mat, S., Sopian, K., Sulaiman, M. Y., & Mohammad, A. T. (2013). Numerical study of PCM solidification in a triplex tube heat exchanger with internal and external fins. *International Journal of Heat and Mass Transfer, 61*(1), 684–695.
13. Vajjha, R. S., Das, D. K., & Namburu, P. K. (2010). International Journal of Heat and Fluid Flow Numerical study of fluid dynamic and heat transfer performance of Al_2O_3 and CuO nanofluids in the flat tubes of a radiator. *International Journal of Heat and Fluid Flow, 31*(4), 613–621.
14. Mahdavi, M., Tiari, S., & Pawar, V. (2020). A numerical study on the combined effect of dispersed nanoparticles and embedded heat pipes on melting and solidification of a shell and tube latent heat thermal energy storage system *27*(September 2019).
15. Prakash, & Voller, V. (1989). On the numerical solution of continuum mixture model equations describing binary solid-liquid phase change. *Numerical Heat Transfer, Part B: Fundamentals, 15*(2), 171–189.
16. Hong, Y., Ye, W., Du, J., & Huang, S. (2019). International journal of heat and mass transfer solid-liquid phase-change thermal storage and release behaviors in a rectangular cavity under

the impacts of mushy region and low gravity. *International Journal of Heat and Mass Transfer, 130*, 1120–1132.
17. Agyenim, F., Eames, P., & Smyth, M. (2009). A comparison of heat transfer enhancement in a medium temperature thermal energy storage heat exchanger using fins. *Solar Energy, 83*(9), 1509–1520.